ISSN impresa 0717-3644
ISSN online 0718-221X

Maderas. Ciencia y tecnología 2025 (27): 28, 1-13

DOI: 10.22320/s0718221x/2025.28

SHRINKAGE EFFECT ON RADIAL AND TANGENTIAL DIRECTION STRESSES IN CYLINDRICAL WOOD PIECES OF *Pinus taeda*♣

Nilson Tadeu Mascia[1,♠]

https://orcid.org/0000-0002-3103-5201

ABSTRACT

Shrinkage is a key factor in generating internal stresses and deformations within wood structures, especially due to the anisotropic nature of wood, which causes direction-dependent stress responses and must be considered to accurately predict the mechanical behaviour of cylindrical elements. However, its influence on the stress distribution in cylindrical wood elements remains insufficiently explored. This study addresses this gap by formulating a theoretical model to evaluate the development of internal stresses resulting from the shrinkage of wood specimens.

Shrinkage was determined based on the stress–strain relationship of a cylindrical piece of wood, in the absence of external forces, within a cylindrical coordinate system. Due to its radial symmetry, the displacement field is a function of the radius, and the angular displacement is null. Assuming constant longitudinal strains, the strain components can be described as a function of Lekhnitskii's reduced strain coefficients and the associated coefficient, denoted by *k*, where the coefficients depend on the material's elastic properties. Thus, the governing equation of the problem becomes a function of the strain coefficients and, consequently, of shrinkage.

To demonstrate the effects of shrinkage and to show how stresses in the radial and tangential directions are influenced, the elastic coefficients of the wood species *Pinus taeda* (loblolly pine) were experimentally obtained, and the coefficient *k* was determined. Overall, the results emphasise the importance of considering shrinkage and anisotropy when evaluating radial and tangential stresses, as well as radial displacements, in cylindrical wood elements.

Keywords: Anisotropic elasticity, compression wood, Lekhnitskii´s coefficients, wood shrinkage.

INTRODUCTION

The purpose of this article is to present the influence of shrinkage on stresses and displacements based on the concepts of anisotropy applied to wood. These concepts are fundamentally rooted in the classic work of Lekhnitskii (1981), which established the foundational principles of general anisotropy. Lekhnitskii's contributions are pivotal in understanding how materials like wood behave under stress, providing the theoretical framework necessary for further exploration of material anisotropy.

Building on this foundation, the seminal study by Hsu and Tang (1974) applied these anisotropy principles specifically to the study of wood shrinkage, making their work essential for analysing shrinkage-induced stresses in wood. Together, these studies form the backbone of the theoretical approach used in this article to explore the relationship between shrinkage and stresses in anisotropic materials such as wood.

The analysis of wood shrinkage in terms of stresses and strains can be performed by considering a cylindrical piece of wood with no external forces acting upon it. This shape reflects the natural form of roundwood

[1]Universidade Estadual de Campinas (UNICAMP). Faculdade de Engenharia Civil. Arquitetura e Urbanismo (FECFAU). São Paulo, Brazil.

♣This article is an extended and peer-reviewed version of the paper presented first at the III Congreso Ibero-Latinoamericano de la Madera en la Construcción (CIMAD), held in Madrid-Spain, June 2024. Associate Editor: Laura Moya

♠Corresponding author: ntm@unicamp.br

Received: 20.08.2024 Accepted: 03.07.2025

elements used in structures such as poles and columns and is referenced in testing standards like EN 14229 (2010). It is also employed in experimental studies to align growth rings and minimise boundary effects (Hsu and Tang 1974). The adoption of this geometry represents a rational simplification that leverages the body's radial symmetry, allowing for the direct application of Lekhnitskii's anisotropic elasticity theory. This approach enables the derivation of closed-form analytical solutions to evaluate the effects of shrinkage, avoiding the need for complex numerical simulations. Although idealised, this geometry facilitates the understanding of stress patterns relevant to curved or layered wood elements in structural applications.

The shrinkage resulting from humidity variation can be computed as strain components, and therefore, from constitutive relations, the associated stresses and displacements can be calculated.

The model developed by Ylinen and Jumppanen (1967), also referenced by Hsu and Tang (1974), was one of the earliest theoretical approaches to wood shrinkage, focusing on linear and volumetric shrinkage along the principal orthotropic directions of wood (longitudinal, radial, and tangential). It is empirical in nature, relying on observed shrinkage behaviour rather than a complete mechanical formulation.

In contrast, the model presented in this study is based on Lekhnitskii's anisotropic elasticity theory and is applied to a cylindrical geometry with radial symmetry. This allows for an analytical evaluation of shrinkage-induced stresses and displacements.

The theoretical model of Lekhnitskii (1981) enables a direct analytical understanding of shrinkage-induced stresses, particularly considering wood's directional behaviour. This approach is especially useful for isolating the effects of anisotropy in a controlled, idealised setting.

Finite element methods have been widely used to analyse shrinkage-induced stresses in wood, particularly under moisture gradients and anisotropic conditions, as shown in the studies by Svensson and Toratti (2002) and Kongyang et al. (2019). While these approaches are powerful for simulating complex geometries and moisture profiles, they require extensive numerical input and calibration. The analytical model proposed in this study offers a complementary alternative for understanding fundamental shrinkage behaviour in an idealised setting.

Thus, compared with finite element analyses, which require meshing, numerical solvers, and extensive calibration, and with empirical shrinkage formulas that rely on species-specific curve fits, the Lekhnitskii-based analytical model offers closed-form solutions that are fast to apply, free from numerical noise, and readily transferable once the elastic compliance matrix of the wood is known.

Because of the radial symmetry associated with the cylindrical shape the displacement field is a function of the radial position r only, where it is assumed that the displacement in the longitudinal direction z is zero, and the deformation is constant. Therefore, the deformations can be described as a function of the reduced coefficients of deformation that were proposed by Lekhnitskii (1981). Note that these coefficients and the associated coefficient, denoted k, depend on the material's elastic properties, constituting the structure or the analysed structural piece.

By accounting for shrinkage in these deformations as components and consequently in the coefficients, it is possible to assess the influence of shrinking in the stresses by analysing the solution of the differential equation containing the deformation coefficients.

In this context, this paper analyses the general framework of Lekhnitskii's theory of anisotropic elasticity, followed by a discussion of how these shrinkage concepts are applied, as outlined by Hsu and Tang (1974). To complement the theoretical analysis, an experimental procedure was conducted to determine the elastic and shrinkage properties of the wood. This procedure included tests to measure the elastic moduli and evaluate the shrinkage coefficients of the wood, which are critical for understanding its behaviour under varying moisture conditions.

Furthermore, an application example is provided, with the aim demonstrating the influence of shrinkage using a cylindrical piece of the reforested wood species loblolly pine (*Pinus taeda* L.) This example highlights how shrinkage impacts stresses, deformations and displacements in wood structures.

This research can also provide valuable insights for the understanding of engineered wood products, such as Glulam and cross-laminated timber (CLT), which are increasingly used in modern construction for their

strength, sustainability, and efficiency, where dimensional stability is critical to maintaining the structural integrity of buildings over time. Both Glulam and CLT, when made from loblolly pine (*Pinus taeda* L.), a reforested wood species prevalent in Brazil (Vilela and Mascia 2021), offer significant advantages in terms of structural performance.

Analysis of shrinkage considering the coefficients of strain reduction

This section, which is based on the studies previously developed by Hashin (1967), Malvern (1969), Gopu and Goodman (1974), Saliklis (1992), and particularly by Lekhnitskii (1981), presents a theoretical conceptualization of the calculations that determine the deformation, displacements, and stresses of a cylindrical body.

Consider a wood log with an approximately cylindrical shape that is extracted from the wood block shown in Figure 1. The six stress components and three displacement projections must be determined to derive the stress and strain distributions to satisfy the equilibrium equations and boundary conditions. In the case of cylindrical anisotropy with an anisotropic axis *z*, the stress and strain in the axial direction can be considered constant.

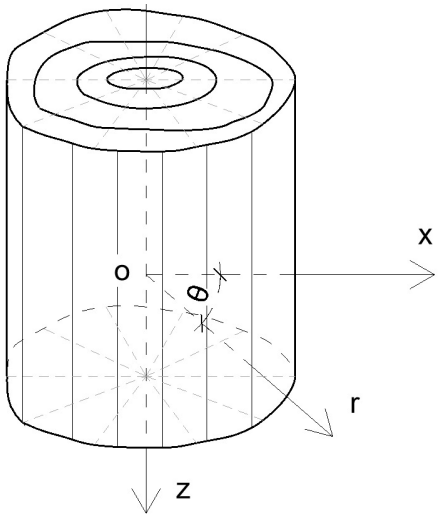

Figure 1: Cylindrical coordinates in a wood block.

Generally, the constitutive relations between the normal σ and tangential τ stresses and the normal ε and tangential γ strains written in expanded index notation are the following Equation 1:

$$\begin{aligned}
\varepsilon_r &= S_{11}\sigma_r + S_{12}\sigma_\theta + S_{13}\sigma_z + S_{14}\tau_{\theta z} + S_{15}\tau_{rz} + S_{16}\tau_{r\theta} \\
\varepsilon_\theta &= S_{12}\sigma_r + S_{22}\sigma_\theta + S_{23}\sigma_z + S_{24}\tau_{\theta z} + S_{25}\tau_{rz} + S_{26}\tau_{r\theta} \\
\varepsilon_z &= S_{13}\sigma_r + S_{23}\sigma_\theta + S_{33}\sigma_z + S_{34}\tau_{\theta z} + S_{35}\tau_{rz} + S_{36}\tau_{r\theta} \\
\gamma_{\theta z} &= S_{14}\sigma_r + S_{24}\sigma_\theta + S_{34}\sigma_z + S_{44}\tau_{\theta z} + S_{45}\tau_{rz} + S_{46}\tau_{r\theta} \\
\gamma_{rz} &= S_{15}\sigma_r + S_{25}\sigma_\theta + S_{35}\sigma_z + S_{45}\tau_{\theta z} + S_{55}\tau_{rz} + S_{56}\tau_{r\theta} \\
\gamma_{r\theta} &= S_{16}\sigma_r + S_{26}\sigma_\theta + S_{36}\sigma_z + S_{46}\tau_{\theta z} + S_{56}\tau_{rz} + S_{66}\tau_{r\theta}
\end{aligned} \qquad (1)$$

Note that the terms S_{ij}, where i,j = 1 to 6, represent the compliance coefficients, which depend on the material's elastic properties under analysis.

Using the normal strain in *z,* equal to *D,* and isolating the normal stress in *z*, results in Equation 2:

$$\sigma_z = \frac{D}{S_{33}} - \frac{1}{S_{33}}\left(S_{13}\sigma_r + S_{23}\sigma_\theta + ... + S_{36}\tau_{r\theta}\right) \quad (2)$$

By applying Equation 1 and Equation 2 according to Lekhnitskii (1981) the reduced coefficients of deformation are defined and written in index notation by Equation 3:

$$\beta_{ij} = S_{ij} - \frac{S_{i3}S_{j3}}{S_{33}} \quad (3)$$

Where $i, j = 1,2,3,4,5,6$. Note that this tensor is symmetric, and $\beta_{i3} = \beta_{3i} = 0$ for *i* =*1* to *6*.

Expressing the constitutive equations using the reduced notation and incorporating the coefficients of reduced deformation β_{ij}, where both *i* and *j* range from 1 to 3, yielding the following Equation 4:

$$\begin{aligned}
\varepsilon_1 &= \beta_{11}\sigma_1 + \beta_{12}\sigma_2 .... + \beta_{16}\tau_{12} + \frac{S_{13}}{S_{33}}\varepsilon_3 \\
\varepsilon_2 &= \beta_{12}\sigma_1 + \beta_{22}\sigma_2 .... + \beta_{26}\tau_{12} + \frac{S_{23}}{S_{33}}\varepsilon_3 \\
\gamma_{12} &= \beta_{14}\sigma_1 + \beta_{24}\sigma_2 .... + \beta_{46}\tau_{12} + \frac{S_{43}}{S_{33}}\varepsilon_3 \\
\gamma_{31} &= \beta_{15}\sigma_1 + \beta_{25}\sigma_2 .... + \beta_{56}\tau_{12} + \frac{S_{53}}{S_{33}}\varepsilon_3 \\
\gamma_{23} &= \beta_{11}\sigma_1 + \beta_{26}\sigma_2 .... + \beta_{66}\tau_{12} + \frac{S_{63}}{S_{33}}\varepsilon_3
\end{aligned} \quad (4)$$

Focusing on the research conducted by Lekhnitskii (1981) and Hsu and Tang (1974), an investigation into wood shrinkage was undertaken, examining a log piece devoid of external forces. The analysis explored how shrinkage induces normal stresses within the wood log. Fridley and Tang (1993) also conducted a three-dimensional analysis following similar guidelines. In this context, the shrinkage components (α_r, α_z and α_θ) are calculated as part of the stress-strain relations in cylindrical coordinates, using Equation 1 for normal stresses and strains, which are simplified to Equation 5:

$$\begin{aligned}
\varepsilon_r &= S_{rr}\sigma_r + S_{r\theta}\sigma_\theta + S_{rz}\sigma_z - \alpha_r; \\
\varepsilon_\theta &= S_{r\theta}\sigma_r + S_{\theta\theta}\sigma_\theta + S_{\theta z}\sigma_z - \alpha_\theta; \\
\varepsilon_z &= S_{rz}\sigma_r + S_{\theta z}\sigma_\theta + S_{zz}\sigma_z - \alpha_z;
\end{aligned} \quad (5)$$

Where ε_r, ε_θ, ε_z represent the strains while σ_r, σ_θ, σ_z represent the stresses according to the adopted cylindrical coordinates (*r* and θ). The terms $S_{rr}, S_{r\theta}, S_{rz}, S_{\theta\theta}, S_{\theta z}$ and S_{zz} denote the compliance tensor related to the wood´s elastic coefficients.

This problem involves the solution of the equilibrium equations for strain and stress distribution of a cylinder under no external load, given knowledge of the wood´s elastic constants and the free linear shrinkage Hsu and Tang (1974).

The values for shrinkage, expressed as percentages, can be found in the following references: Zenid (2003) and Trianoski *et al.* (2013) for national wood species and Bodig and Jayne (1982) for foreign species. The Brazilian Association of Technical Standards, ABNT NBR 7190-3 (2022), establishes the procedures to evaluate the dimensional stability of wood orthotropy.

Due to radial symmetry, the displacement field is a function of r, and the displacement in the θ-direction is zero. Therefore, the strains are Equation 6:

$$\varepsilon_r = \frac{\partial u_r}{\partial r}; \varepsilon_\theta = \frac{u_r}{r}; \varepsilon_z = \frac{\partial u_z}{\partial z} = c \quad (6)$$

Where c is a constant.

Now, considering the reduced coefficients of deformation as presented in Equation 4 and using Equation 5 for cylindrical coordinates, noting that the strain in z is constant equal to c, the following relations can be written Equation 7:

$$\varepsilon_r = \beta_{rr}\sigma_r + \beta_{r\theta}\sigma_\theta + \beta_r; \varepsilon_\theta = \beta_{r\theta}\sigma_r + \beta_{\theta\theta}\sigma_\theta + \beta_\theta \quad (7)$$

And the following equations in the terms of β_{ij} are obtained Equation 8:

$$\beta_{rr} = S_{rr} - \frac{S_{rz}S_{rz}}{S_{zz}}; \beta_{\theta\theta} = S_{\theta\theta} - \frac{S_{\theta z}S_{\theta z}}{S_{zz}}; \beta_{r\theta} = S_{r\theta} - \frac{S_{rz}S_{\theta z}}{S_{zz}}; \beta_\theta = \frac{S_{\theta z}}{S_{zz}}\left(c + \alpha_z\right) - \alpha_\theta; \beta_r = \frac{S_{rz}}{S_{zz}}\left(c + \alpha_z\right) - \alpha_r \quad (8)$$

The equilibrium equation requires that Equation 9:

$$\frac{\partial \sigma_r}{\partial r} + \frac{\sigma_r - \sigma_\theta}{r} = 0 \quad (9)$$

With this, the problem to be solved depends on determining the solution to this equation, the constitutive equations, and the strain compatibility equation (Ting 1996). It is therefore assumed that a function F(r) that is differentiable in r exists such that Equation 10:

$$\sigma_r = \frac{F'}{r}; \sigma_\theta = F'' \quad (10)$$

Note that Equation 10 satisfies the equilibrium equation (Equation 9). Substituting Equation 10 into Equation 7, the following is obtained Equation 11:

$$\varepsilon_r = \beta_{rr}\frac{F'}{r} + \beta_{r\theta}F'' + \beta_r; \varepsilon_\theta = \beta_{r\theta}\frac{F''}{r} + \beta_{\theta\theta}F'' + \beta_\theta \quad (11)$$

Substituting these strains into the compatibility Equation 12:

$$r\frac{d^2\varepsilon_\theta}{dr^2}+2\frac{d\varepsilon_\theta}{dr}-\frac{d\varepsilon_r}{dr}=0 \quad (12)$$

Leads to Equation 13:

$$\beta_{\theta\theta}\left(\frac{d^4F}{dr^4}+\frac{2d^3F}{rdr^3}\right)+\beta_{rr}\left(-\frac{1d^2F}{r^2dr^2}+\frac{1dF}{r^3dr}\right)=0 \quad (13)$$

The general form of the solution to this differential equation is the following Equation 14:

$$F=\frac{A_1}{2}r^2+\frac{A_2}{1+k}r^{1+k}+\frac{A_3}{1-k}r^{1-k}+A_4 \quad (14)$$

The stresses are now determined and are equal to Equation 15**.**

$$\sigma_r=A_1+A_2r^{k-1}+A_3r^{-k-1};\sigma_\theta=A_1+A_2kr^{k-1}-A_3kr^{-k-1} \quad (15)$$

Where there are three unknown constants and $k=\sqrt{\frac{\beta_{rr}}{\beta_{\theta\theta}}}$. Hsu and Tang (1974) assumed that the inner part of the tree log consists of low-density material. Disregarding this part, the tree log becomes a cylinder with an internal cavity. Hence, the displacement should be zero at the centre of the cylinder. As long as *k*, in general, is greater than zero, then u_r at *r* is equal to zero, and A_3 becomes zero. Additionally, because the deformations are continuous (in *r* equal to zero), $\varepsilon_\theta-\varepsilon_r+r\frac{d\varepsilon_\theta}{dr}=0.$

With this, A_1 can be determined by Equation 16:

$$A_1=\frac{\beta_r-\beta_\theta}{\beta_{\theta\theta}-\beta_{rr}} \quad (16)$$

Since there are no external loads at r = R, the stress is zero, which implies that $A_2=-\frac{A_1}{R^{k-1}}$. Then, the stresses and radial displacement become Equation 17:

$$\sigma_r=A_1\left(1-\frac{r^{k-1}}{R^{k-1}}\right);\sigma_\theta=A_1\left(1-\frac{k\ \ r^{k-1}}{R^{k-1}}\right);u_r=\varepsilon_\theta r=\left[\beta_{r\theta}\sigma_r+\beta_{\theta\theta}\sigma_\theta+\beta_\theta\right]r \quad (17)$$

Finally, the constant *c*, which appears in Equation 8, is determined due to the non-existent loads external to the stress at the top or base of the cylinder, and thus $2\pi\int_0^R\sigma_z r dr=0$, resulting in Equation 18:

$$c = \frac{\beta_r - \beta_\theta}{\beta_{\theta\theta} - \beta_{rr}} \left[\left(S_{rz} + S_{\theta z} \right) - \frac{2\left(S_{rz} + kS_{\theta z} \right)}{k+1} \right] - \alpha_z \quad (18)$$

In the case of isotropy, $\alpha = \alpha_\theta = \alpha_z$, and if $k = 1$, then $\sigma_r = \sigma_\theta = 0$.

Observe that the coefficient k depends on β_{ij} which, in turn, is influenced by the wood´s elastic properties and requires experimental determination for each wood species. To provide an illustration, Table 1 presents some k-values for a humidity content of 12 %, which is the standard value typically adopted in normative contexts and was maintained during the experimental part of this study.

Table 1: Coefficient k values for different wood species.

Wood species	k
Green ash *	0,761
Yellow-poplar*	0,678
Pinus caribaea**	0,865

*Hsu and Tang (1974),** Mascia (2015).

MATERIALS AND METHODS

Specimens and experimental procedure

The wood species used in the tests was loblolly pine (*Pinus taeda* L.). The wood blocks, approximately 50 cm in diameter, from which the compression test specimens were extracted, were obtained from local sawmills and conditioned in a laboratory environment at a temperature of 25 °C and a relative humidity of around 65%. After the moisture content was stabilized, the specimens were cut and prepared for testing at a moisture content (MC) of approximately 12%.

In this study, the influence of moisture is incorporated implicitly. Moisture effects were handled implicitly in the modelling. All elastic coefficients were evaluated on these uniformly conditioned specimens (12 % MC), and shrinkage strains were calculated for a uniform moisture drop from the fibre-saturation point (~30 % MC) to 12 % MC. No spatial moisture gradient was modelled; this choice isolates the mechanical influence of anisotropy under homogeneous drying.

From a wood block with growth rings that are approximately cylindrical surfaces, specimens were extracted to determine the wood´s elastic properties (Figure 2) required for calculating the coefficient *k.*

Subsequently, the specimens were tested in each direction, following the presented scheme, with the following dimensions: 4 cm x 4 cm x 10 cm. Electrical KYOWA strain gauges were employed, labelled KFC-5-C1-11, with a length of 5 mm, a gauge factor of 2,10 and an electrical resistance of 120 Ω to obtain the deformations, and an AMSLER universal testing machine with a 250-kN capacity provided the loads.

Six smaller pieces were extracted from inside the block, aligned with the r, θ, and z directions, as well as with the respective planes r–θ, z–r, and z–θ. Two additional repetitions were carried out following this same scheme, totalling 18 test specimens. This sampling procedure follows the guidelines established by the Brazilian standard ABNT NBR 7190:2022.

Due to the wood block´s diameter of approximately 50 cm, these specimens were smaller than those typically used for simple compression tests for non-native species, as indicated in the Brazilian standard ABNT NBR 7190-2 (2022). The θ direction is adopted as illustrated in Figure 2, oriented as closely as possible with the cylindrical coordinate system.

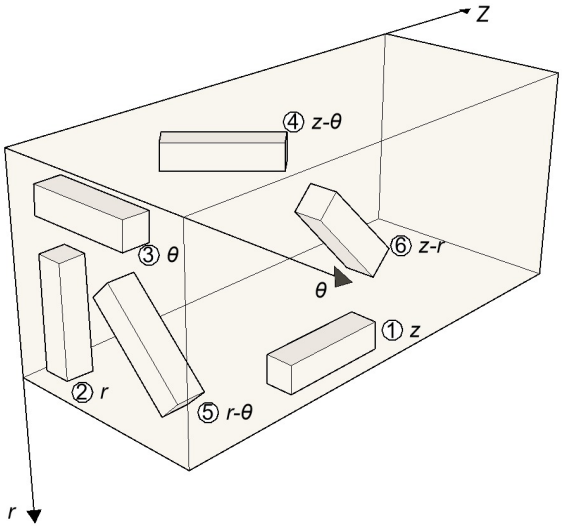

Figure 2: Wood block with specimens.

Legend - Specimens: 1-oriented in the *z*-direction; 2-oriented in the *r*-direction; 3-oriented in the *θ*-direction;4-oriented in the z-θ plane at an angle of approximately 45°; 5- oriented in the *r*-*θ* plane at an angle of approximately 45°; 6-oriented in the *z*-*r* plane at an angle of approximately 45°.

The use of loblolly pine (*Pinus taeda* L.) in this experimental procedure not only supports sustainable forest management but also aligns with global trends toward eco-friendly and carbon-neutral construction methods. Additionally, loblolly pine (*Pinus taeda* L.) fast growth and adaptability make it an economical choice for Brazil's timber industry, further promoting the use of engineered wood in both domestic and international markets.

Thus, from the specimen oriented in the z-direction (Specimen 1), the following coefficients for Poisson's ratios and elastic modulus in this direction were obtained in Equation 19:

$$\nu_{zr} = \frac{\varepsilon_r}{\varepsilon_z}; \nu_{z\theta} = \frac{\varepsilon_\theta}{\varepsilon_z}; E_z = \frac{\sigma_z}{\varepsilon_z} \quad (19)$$

Similarly, other coefficients were obtained from the piece oriented in the *r*-direction (Specimen 2) and the θ-direction (Specimen 3). From the existing symmetry conditions of the coefficients of elasticity (Bodig and Jayne 1982), the following can be derived Equation 20:

$$\frac{\nu_{zr}}{E_z} = \frac{\nu_{rz}}{E_r}; \frac{\nu_{\theta r}}{E_\theta} = \frac{\nu_{r\theta}}{E_r}; \frac{\nu_{z\theta}}{E_z} = \frac{\nu_{\theta z}}{E_\theta} \quad (20)$$

The shear elastic modulus was determined using specimens 4, 5 and 6 through coordinate transformations at an angle of approximately 45°. It is important to note that in a coordinate system where axial compressive loading coincides with one of the principal directions (z, r and *θ*), it is not possible to determine the shear elastic modulus, as this involves tangential stresses and strains (distortions). To enable determination, the stress-strain relationship must be equated in a plane with principal directions not coinciding with the direction of the compressive load, and specimens must be prepared with principal directions not coinciding with the direction of the applied load according to Mascia and Nicolas (2013).

Figure 3 illustrates the positioning of the strain gauges for the case of the *r* and *θ* directions (specimen 5), as well as at 45°, referred to as direction 1, and orthogonal to this, direction 2, where a strain gauge is placed

to measure the Poisson's ratio concerning axes 1 and 2. The procedure is analogous for the other directions, *z* and *r* (specimen 4) , and *z* and θ (specimen 6).

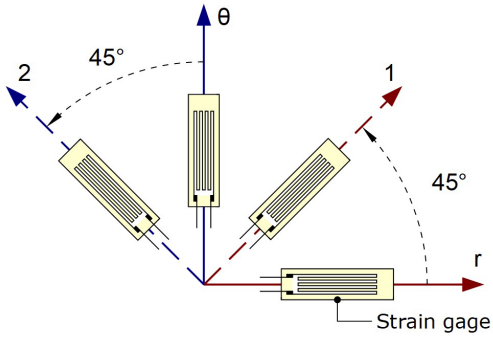

Figure 3: Strain gages and related directions.

Table 2 presents the results for the overall elastic characterisation of this wood species sample.

Table 2: Mean values of the coefficients of elasticity.

$E_z = 18200$ MPa	$E_\theta = 301$ MPa	$E_r = 452$ MPa
$G_{rz} = 390$ MPa	$G_{r\theta} = 110$ MPa	$G_{z\theta} = 280$ MPa
$\nu_{rz} = 0{,}013$	$\nu_{r\theta} = 0{,}539$	$\nu_{\theta z} = 0{,}005$

Considering a system in cylindrical coordinates aligned with the main directions of elasticity, *k* is calculated as $\sqrt{\frac{\beta_{rr}}{\beta_{\theta\theta}}}$ with the participating terms of *k* (Lekhnitskii 1981) given by Equation 21:

$$\begin{aligned}
\beta_{rr} &= S_{rr} - \frac{S_{rz}S_{rz}}{S_{zz}} = \frac{1}{E_r} - \frac{\nu_{rz}^2}{E_r};\\
\beta_{\theta\theta} &= S_{\theta\theta} - \frac{S_{\theta z}S_{\theta z}}{S_{zz}} = \frac{1}{E_\theta} - \frac{\nu_{\theta z}^2}{E_\theta};\\
\beta_r &= \frac{S_{rz}}{S_{zz}}\left(c+\alpha_z\right) - \alpha_r = -\nu_{z\theta}\left(c+\alpha_z\right) - \alpha_r;\\
\beta_\theta &= \frac{S_{\theta z}}{S_{zz}}\left(c+\alpha_z\right) - \alpha_\theta = -\nu_{z\theta}\left(c+\alpha_z\right) - \alpha_\theta
\end{aligned} \qquad (21)$$

Note that the terms S_{ij} represent the compliance coefficients and β_{ij} are the Lekhnistkii´s reduced coefficients of deformation, for *i,j* = *r, z* and θ. From these relations, the mean value found for *k* is 0,865.

Finally, Trianoski *et al.* (2013) assessed the shrinkage properties for varying humidity in the wood from 30 % down to 12 %, yielding mean values of $\alpha_\theta = 0{,}06; \alpha_r = 0{,}03; \alpha_z = 0{,}001$.

It should be noted that Lekhnitskii's reduced coefficients of deformation depend on the elastic coefficients, which are determined through laboratory tests on specimens, where strains are measured. The stresses are then calculated based on these reduced coefficients, the *k* parameter, and the geometry of the cylindrical piece.

RESULTS AND DISCUSSION

Calculations of the stresses and radial displacements

Based on the values obtained from the experimental results (Table 2), graphs are plotted showing the stresses and displacements in the radial and tangential directions (Halsenman and Littlefield 1999). In this context, shrinkage (α_i) is computed as part of the stresses and deformations relations.

Next, the parameters used for creating Figure 4 is displayed, showing variations of stress in *r* (the radial direction) σ_r and in θ (the tangential direction) σ_θ , from the centre of a wood piece toward the border, i.e., the *r* coordinate ranging from 0 to *R*. Figure 5 shows the radial displacements.

The terms β_r and β_θ and *c* depend on the elastic coefficients and shrinkage values. Thus Equation 22:

$$\beta_{rr} \approx 2,21x10^{-4}; \beta_{\theta\theta} \approx 3,32x10^{-4}; \beta_r = \approx -0,03; \beta_\theta \approx -0,06 \quad (22)$$

Table 3 summarises these calculations:

Table 3: Mean

β_{rr}	$2,21x10^{-4}$
$\beta_{\theta\theta}$	$3,32x10^{-4}$
β_r	$-0,03$
β_θ	$-0,06$

values of Lekhnitskii´s reduced coefficients of deformation.

Consequently with $k = 0,8156,\ A_1 = \dfrac{\beta_r - \beta_\theta}{\beta_{\theta\theta} - \beta_{rr}} \approx 27,02,$ the stresses become Equation 23:

$$\sigma_r = A_1\left(1 - \frac{r^{k-1}}{R^{k-1}}\right); \sigma_\theta = A_1\left(1 - \frac{kr^{k-1}}{R^{k-1}}\right) \quad (23)$$

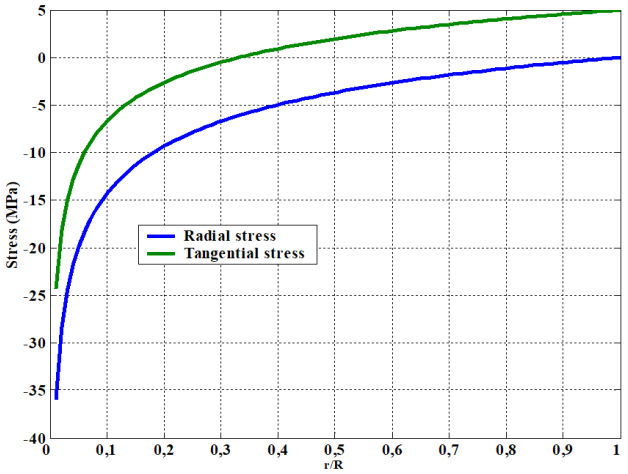

Figure 4: Radial and tangential stresses from the centre toward the border of the wood piece.

Figure 4 illustrates that the radial stress increases from the border to the centre of the piece, reaching a maximum compression value of approximately 36 MPa. In the tangential direction, there is a tensile stress of 5 MPa at the borders, while at the centre, the stress reaches a maximum compression of 25 MPa. These resulting stresses may surpass the average compressive or tensile strength of loblolly pine (*Pinus taeda* L.) (typically between 30 MPa and 60 MPa) and become even more critical when acting in tension perpendicular to the grain, where mean strength values are around 28 MPa (Mustefaga *et al*. 2019, ABNT NBR 7190-1 2022).

In Figure 5, the maximum radial displacement reaches 1,3 cm at the borders in relation to the centre of the piece. Thus, the use of this type of analysis in metal plate manufacturing practices, such as gangnails (O'Regan and Woeste 2002) or stainless steel (Corradi *et al*. 2019), is essential for wood pieces, as it helps to reduce such stresses and, consequently, the resulting deformations and displacements.

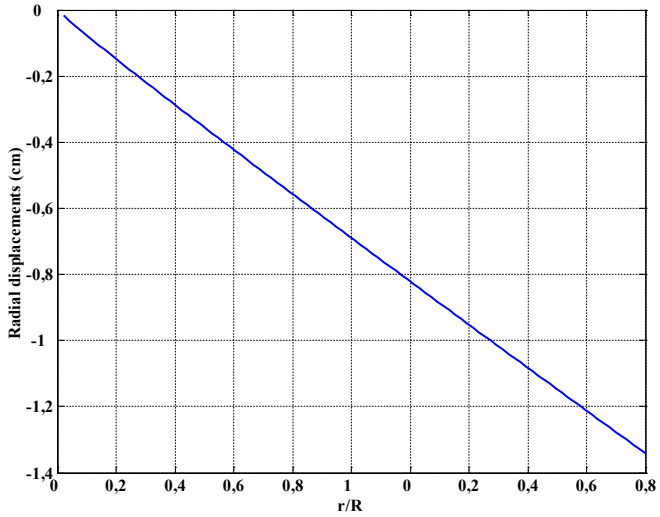

Figure 5: Radial displacement from the centre toward the border of the wood piece.

It is important to note that the formulation adopted in this research is based on a linear elastic model. The values of the elastic properties used to calculate stresses and displacements were obtained from test specimens that, due to the dimensions of the wood blocks extracted from logs, do not strictly align with the axes of the cylindrical coordinate system assumed in the theoretical model. However, these limitations do not invalidate the adopted procedure, and the results obtained remain consistent with the experimental approach applied to a material with mechanical characteristics such as wood.

CONCLUSIONS

This article presents a study on the analysis of stresses in a wood piece, considering the influence of shrinkage on these stresses and displacements, under the concepts of cylindrical anisotropy. To conduct the analysis, it was necessary to determine a parameter, *k*, which depends on the results of the wood´s elastic properties. These properties were assessed through compression tests on specimens of the loblolly pine (*Pinus taeda* L.) species.

The significance of investigating the influence of shrinkage, especially regarding wood's susceptibility to humidity variations and its association with ruptures and cracks, highlights the need to understand stresses caused by dimensional variations in wood, which can help prevent fissures and ensure its proper use in structural designs.

It was observed that during shrinkage, stresses in the tangential direction may lead to tensile ruptures, causing fissures in the piece, which is detrimental for wood structures.

In many cases, these stresses can exceed the compressive or tensile mean strength of loblolly pine (*Pinus taeda* L.), or, even more critically, when associated with tension perpendicular to the grain, where the material is most vulnerable.

The model used in this study is limited by its linear elastic assumptions and dependence on species-specific properties. As it was calibrated for *Pinus taeda*, applying it to other wood species would require new experimental data. Nonetheless, this limitation is consistent with the model's theoretical scope.

It is worth noting that the results indicate that wood anisotropy is an essential factor to be considered in the generation and distribution of shrinkage-induced stresses. The direction-dependent mechanical behaviour of wood influences both the magnitude and pattern of internal stresses and deformations, especially in cylindrical geometries. This highlights the relevance of adopting an anisotropic elasticity framework, such as Lekhnitskii's model, to better describe and interpret the mechanical behaviour of wood under shrinkage effects.

While the model does not aim to simulate cross-laminated timber (CLT) elements directly, it provides valuable reference values and insight into directional shrinkage effects, particularly relevant to layered engineered wood products. These findings support a better understanding of the behaviour of structural elements like CLT and Glulam made from *Pinus taeda*, a commonly used reforested species in Brazil, and contribute to improvements in the design and manufacturing processes of sustainable wood-based construction.

Authorship contributions

N. T. M.: Conceptualisation, formal analysis, methodology, investigation, funding acquisition, writing - review & editing.

Acknowledgements

The author would like to thank the São Paulo Research Foundation, FAPESP (Process n. 2014/23818-1, titled "Study of elastic and strength parameters of wood to use in the glued laminated timber beams") and the Brazilian National Council for Scientific and Technological Development, CNPq (Processes n. 307202/2019-4,titled "Numerical and experimental analysis of cross laminated timber (CLT) plates subject to bending" and n.305363/2022-0, titled "Experimental and numerical analysis of cross laminated timber and concrete composite plates") for their financial support for this research.

REFERENCES

ABNT. 2022a. Projeto de estruturas de madeira – Parte 1: Critérios de dimensionamento. ABNT NBR 7190-1. ABNT: Rio de Janeiro, Brasil.

ABNT. 2022b. Projeto de estruturas de madeira – Parte 2: Métodos de ensaio para classificação visual e mecânica de peças estruturais de madeira. ABNT NBR 7190-2. ABNT: Rio de Janeiro, Brasil.

ABNT. 2022c. Projeto de estruturas de madeira – Parte 3: Métodos de ensaio para corpos de prova isentos de defeitos para madeiras de florestas nativas. ABNT NBR 7190-3. ABNT: Rio de Janeiro, Brasil.

Bodig, J.; Jayne, B.A. 1982. *Mechanics of wood and wood composites*. Krieger Publishing Company: Florida, USA. ISBN 9780898745370. 712p.

Corradi, M.; Adelaja, I.O.; Borri, A. 2019. Repair and reinforcement of historic timber structures with stainless steel. *Metals* 9(1). e106. https://doi.org/10.3390/met9010106

European Committee for Standardization. 2010. Structural round timber – Requirements for visual grading of softwood. EN 14229. CEN: Brussels, Belgium. https://www.en-standard.eu/eurocodes

Fridley, K.J.; Tang, R.C. 1993. Modelling three-dimensional distortion of wood due to anisotropic shrinkage. *Mathematical and Computer Modelling* 17(9): 23–30. https://doi.org/10.1016/0895-7177(93)90014-P

Gopu, V.K.A.; Goodman, J.R. 1974. Analysis of double-tapered pitched and curved laminated beam section. *Wood Science* 7(1): 52–60.

Halsenman, D.; Littlefield, B. 1999. *Matlab 5 – Versão do estudante: guia do usuário*. Makron Books: São Paulo, Brasil. ISBN 9788534606566. 320p.

Hashin, Z. 1967. Plane anisotropic beams. *Journal of Applied Mechanics* 34(2): 257-262. https://doi.org/10.1115/1.3607676

Kongyang, C.; Hongxing, Q.; Menglin, S.; Frank, L. 2019. Experimental and numerical study of moisture distribution and shrinkage crack propagation in cross section of timber members. *Construction and Building Materials* 221: 219–231. https://doi.org/10.1016/j.conbuildmat.2019.05.191

Hsu, N.N.; Tang, R.C. 1974. Internal stresses in wood logs due to anisotropic shrinkage. *Wood Science* 7(1): 43–51.

Lekhnitskii, S.G. 1981. *Theory of elasticity of an anisotropic body*. Mir Publishers: Moscow, Russia. ISBN 9780828522409. 320p.

Malvern, L.E. 1969. *Introduction to the mechanics of a continuous media*. Prentice-Hall International: London, UK. ISBN 9780134876030. 713p.

Mascia, N.T. 2015. Análise de tensões e deslocamentos em peças cilíndricas de madeira devido à retração. *Matéria* 20(1): 32–46. https://doi.org/10.1590/S1517-707620150001.0007

Mascia, N.T.; Nicolas, E.A. 2013. Determination of Poisson's ratios in relation to fiber angle of a tropical wood species. *Construction and Building Materials* 41: 691–696. https://doi.org/10.1016/j.conbuildmat.2012.12.014

Mustefaga, E.C.; Hillig, E.; Tavares, E.L.; Sozim, P.C.L.; Rusch, F. 2019. Caracterização físico-mecânica da madeira juvenil de *Pinus*. *Scientia Forestalis* 47(123): 472–481. https://doi.org/10.18671/scifor.v47n123.09

O'Regan, P.J.; Woeste, F.E. 2002. Withdrawal strength of punched metal tooth plates in red oak end grain. *Forest Products Journal* 52(10): 82–88.

Saliklis, E. 1992. *A nonlinear constitutive model of paperboard*. PhD Thesis. University of Wisconsin-Madison. 246p.

Svensson, S.; Toratti, T. 2002. Mechanical response of wood perpendicular to grain when subjected to changes of humidity. *Wood Science and Technology* 36: 145–156. https://doi.org/10.1007/s00226-001-0130-4

Ting, T.C.T. 1996. *Anisotropic elasticity: theory and applications*. Oxford University Press: New York, USA. ISBN 9780195074478. 573p.

Trianoski, R.; Matos, J.M.; Iwakiri, S.; Prata, J.G. 2013. Avaliação da estabilidade dimensional de espécies de *Pinus* tropicais. *Floresta e Ambiente* 20(3): 398–406. http://dx.doi.org/10.4322/floram.2012.071

Vilela, R.T.; Mascia, N.T. 2021. Avaliação de propriedades mecânicas da madeira de *Pinus taeda* provenientes de placas de cross-laminated timber. *Ambiente Construído* 21(4): 89–110. https://doi.org/10.1590/s1678-86212021000400560

Ylinen, A.; Jumppanen, P. 1967. Theory of the shrinkage of wood. *Wood Science and Technology* 1(4): 241–252.

Zenid, G.J. 2003. *Madeira: uso sustentável na construção civil*. Instituto de Pesquisas Tecnológicas (IPT): São Paulo, Brasil. https://madeiras.ipt.br/madeira-uso-sustentavel-na-construcao-civil/